UC Berkeley
UC Berkeley Previously Published Works

Title

Development of sensitivity analysis capabilities of generalized responses to nuclear data in Monte Carlo code RMC

Permalink

https://escholarship.org/uc/item/3vt4h5xd

Authors

Qiu, Yishu
Aufiero, Manuele
Wang, Kan
et al.

Publication Date

2016-11-01

DOI

10.1016/j.anucene.2016.07.016

Peer reviewed

CrossMark

Development of sensitivity analysis capabilities of generalized responses to nuclear data in Monte Carlo code RMC

Yishu Qiu [a,b,*], Manuele Aufiero [b], Kan Wang [a], Massimiliano Fratoni [b]

[a] Department of Engineering Physics, Tsinghua University, Beijing 100084, China
[b] Department of Nuclear Engineering, University of California, Berkeley, CA 94720-1730, USA

A B S T R A C T

Capabilities for nuclear data sensitivity and uncertainty analysis have been recently implemented in numerous continuous-energy Monte Carlo codes, including the Reactor Monte Carlo (RMC) code. Previous work developed the capability for RMC of computing sensitivity coefficients of the effective multiplication factor and related uncertainties, due to nuclear data. In this work, such capability was extended to generalized responses in the form of ratios of linear response functions of the forward flux based on the collision history-based approach as implemented in SERPENT2. The superhistory algorithm was also adopted in RMC to reduce memory consumption for generalized sensitivity calculations. These new capabilities of RMC were verified by comparing results of TSUNAMI-1D in SCALE6.1 code package, and SERPENT2 through Jezebel, Flattop and the UAM TMI PWR pin cell benchmark problems.

© 2016 Elsevier Ltd. All rights reserved.

1. Introduction

In the past several years, there has been an increasing interest in performing sensitivity and uncertainty analysis with continuous-energy Monte Carlo codes. Several codes, including MCNP6 (Kiedrowski and Brown, 2013), SERPENT2 (Aufiero et al., 2015), the continuous-energy (CE) version of TSUNAMI-3D (Perfetti and Rearden, 2013) in SCALE6.2, MONK10 (Baker et al., 2015), McCARD (Shim and Kim, 2011), TRIPOLI4 (Truchet et al., 2015), and MORET5 (Jinaphanh et al., 2015), have developed capabilities of computing sensitivity coefficients of the effective multiplication factor with regard to nuclear data. Furthermore, some of these Monte Carlo codes—for example SERPENT2 (Aufiero et al., 2015) and CE-TSUNAMI-3D (Perfetti and Rearden, 2014)—have developed capabilities of computing generalized sensitivity coefficients based on different methods. As known, estimating generalized sensitivity coefficients requires two terms: the direct term which describes the perturbations of nuclear data to the response function, and the indirect term which describes the perturbations of nuclear data to flux or spectrum. Calculating the direct term is relatively easy, whereas computing the indirect term usually requires introducing generalized perturbation theory (GPT). CE-TSUNAMI-3D uses the GEAR-MC method (Perfetti and Rearden, 2014); such method further divides the indirect term into two terms: (1) the intra-generational term that describes how much importance a neutron produces in the current generation until its disappearance; (2) the inter-generational term that describes how much importance a neutron generates in the future generations (Perfetti and Rearden, 2014). Since the inter-generation term is computed using the iterated fission probability (IFP) method (Kiedrowski and Brown, 2013), the GEAR-MC method faces the challenge of huge memory requirements. Rather than solving the generalized perturbation equation explicitly, SERPENT2 uses the collision history-based method applying the concept of accepted and rejected events. Such method takes advantage of the Monte Carlo method itself and is relatively easy to implement.

In previous work, the Reactor Monte Carlo (RMC) code (Wang et al., 2015) acquired the capability of computing sensitivity coefficients of the effective multiplication factor with regard to nuclear data (Qiu et al., 2015). In this work, such capability of RMC was extended to generalized responses based on the collision history-based method (Aufiero et al., 2015) with the major difference that the collision history-based method implemented in SERPENT2 is based on delta-tracking technique, whereas the implementation in RMC is based on the ray-tracking technique. Furthermore, RMC relies on the superhistory algorithm (Qiu et al., 2016) to reduce memory consumption for the generalized sensitivity calculations. Section 2 of this manuscript presents the underlying theory for the collision history-based method, Section 3 describes the superhistory algorithm, and Section 4 provides a comparison of

the results obtained using these newly-developed features in RMC with results of TSUNAMI-1D in SCALE6.1 code package (Oak Ridge National Laboratory, 2011) and SERPENT2 in three different benchmark problems.

2. Methodology

2.1. Generalized sensitivity coefficients

The sensitivity coefficient function is defined as the relative change in the response function, for example the effective multiplication factor divided by the relative change in nuclear data, and is expressed as

$$S_x^R = \frac{\delta R/R}{\delta x/x}, \tag{1}$$

where R is any kind of response functions and x is any nuclear data including microscopic cross sections, nubar, or scattering or fission energy transfer functions, etc.; x is in general function of position $\vec{r}$, incident and outgoing direction $\vec{\Omega}$ and $\vec{\Omega}'$, incident and outgoing energy E and E'. The energy-resolved sensitivity coefficients computed in this work are energy bin-integrated, in the form of

$$S_{x,g}^R = \int_{E_g}^{E_{g-1}} S_x^R(E) dE, \tag{2}$$

where g is the energy bin index and E_g and E_{g-1} are the lower and upper energies, respectively, in bin g. The energy-integrated sensitivity coefficients can be expressed in the form of

$$S_x^R = \int_0^\infty S_x^R(E) dE. \tag{3}$$

It should be noted that for microscopic cross sections and nubar, sensitivity coefficients are usually integrated over incident energy, whereas for scattering and fission energy transfer functions sensitivity coefficients are conventionally integrated over outgoing energy. Furthermore, for scattering transfer functions, sensitivity coefficients can also be expressed as a function of incident energy (also suitable for fission χ transfer function) and scattering cosine. In this work, the linear response function is assumed of the following form

$$R = \frac{\langle \Sigma_1, \Psi \rangle}{\langle \Sigma_2, \Psi \rangle}, \tag{4}$$

where Ψ is the neutron flux, Σ_1 and Σ_2 are any kind of macroscopic cross sections, and $\langle \ \rangle$ is an inner product over phase space. Using generalized sensitivity coefficients, one can conduct sensitivity and uncertainty analysis to different types of response functions. For example, setting $\Sigma_2 = 1$ allows to calculate sensitivity coefficients of one-group cross section obtained by Monte Carlo transport calculations, and these coefficients can be further used to study uncertainty propagation (Park et al., 2011) in depletion calculations. In this work, methods are restricted to first order perturbation theory; therefore, the perturbation of generalized response, δR, caused by perturbations of cross sections can be expressed as

$$\delta R = \left\langle \frac{\frac{d\Sigma_1}{dx}\Psi}{\Sigma_1\Psi} R\delta x - \frac{\frac{d\Sigma_2}{dx}\Psi}{\Sigma_2\Psi} R\delta x + \frac{\partial R}{\partial \Psi}\frac{\partial \Psi}{\partial x}\delta x \right\rangle. \tag{5}$$

Substituting Eq. (5) into Eq. (1), generalized response sensitivity coefficients can be expressed as

$$S_x^R = \left\langle \frac{\frac{d\Sigma_1}{dx}\Psi x}{\Sigma_1\Psi} - \frac{\frac{d\Sigma_2}{dx}\Psi x}{\Sigma_2\Psi} + \frac{\partial R}{\partial \Psi}\frac{\partial \Psi}{\partial x}\frac{x}{R} \right\rangle. \tag{6}$$

The first two terms on the right hand side of Eq. (6) are called the direct effect terms, which describe the impact of perturbations of cross sections on the generalized response. Scoring the direct effect terms in Monte Carlo transport calculations is relative easy to implement and can use standard Monte Carlo tally techniques (X-5 Monte Carlo Team, 2003). Considering the track length estimator, for example, a score for $\langle \Sigma_1 \Psi \rangle$ is equal to

$$\langle \Sigma_1 \Psi \rangle = \frac{1}{C_{tot}} \sum_{c=1}^{C_{tot}} \frac{1}{P_c w_0^c} \sum_{p=1}^{P_c} \sum_{\tau=1}^{L^{p,c}} \Sigma_1 \cdot w_\tau^{p,c} \cdot l_\tau^{p,c}, \tag{7}$$

where c is cycle index, C_{tot} is the total number of active cycles, p is particle index in cycle c, P_c is the total number of particles in cycle c, w_0^c is initial weight of every particle in cycle c, τ is track index for particle p in cycle c, $L^{p,c}$ is total number of tracks for particle p in cycle c, and $w_\tau^{p,c}$ and $l_\tau^{p,c}$ are the current weight and track length of particle p at track τ in cycle c; and a score for $\langle \frac{\partial \Sigma_1}{\partial x} \Psi x \rangle$ is given by

$$\left\langle \frac{\partial \Sigma_1}{\partial x} \Psi x \right\rangle = \frac{1}{C_{tot}} \sum_{c=1}^{C_{tot}} \frac{1}{P_c w_0^c} \sum_{p=1}^{P_c} \sum_{\tau=1}^{L^{p,c}} N_1 \cdot x \cdot \delta_{\sigma_1,x} \cdot w_\tau^{p,c} \cdot l_\tau^{p,c}, \tag{8}$$

where $\Sigma_1 = N_1\sigma_1$, N_1 is the number density, σ_1 is a microscopic cross section, $\delta_{\sigma_1,x}$ is the delta function and equals to one when $\sigma_1 = x$ or σ_1 contains x and zero otherwise. The last term in Eq. (6) is known as the indirect effect term, which describes the impact of perturbations of cross sections on the flux and can be computed by

$$\left\langle \frac{\partial R}{\partial \Psi}\frac{\partial \Psi}{\partial x}\frac{x}{R} \right\rangle = \frac{\left\langle \frac{\partial \Psi}{\partial x}\Sigma_1 x \right\rangle}{\langle \Sigma_1 \Psi \rangle} - \frac{\left\langle \frac{\partial \Psi}{\partial x}\Sigma_2 x \right\rangle}{\langle \Sigma_2 \Psi \rangle}. \tag{9}$$

Scoring the indirect term is more complicated than the direct effect term. TSUNAMI-3D in SCALE6.2 uses the GEAR method (Perfetti and Rearden, 2014) that is based on the generalized perturbation theory to compute the indirect term. SERPENT2 uses the collision-based history method based on the concept of accepted and rejected events (Aufiero et al., 2015) without relying on GPT.

2.2. Collision history-based method

According to Eq. (9), the key to compute the indirect term is to obtain scores for the numerators on the right hand side. Still taking the track length estimator as an example, one can obtain

$$\left\langle \frac{\partial \Psi}{\partial x}\Sigma_1 x \right\rangle = \frac{1}{C_{tot}} \sum_{c=1}^{C_{tot}} \frac{1}{P_c w_0^c} \sum_{p=1}^{P_c} \sum_{\tau=1}^{L^{p,c}} \Sigma_1 \cdot \frac{\partial w_\tau^{p,c}/w_\tau^{p,c}}{\partial x/x} \cdot w_\tau^{p,c} \cdot l_\tau^{p,c}. \tag{10}$$

In order to compute the relative change of particle weight $\partial w_\tau^{p,c}/w_\tau^{p,c}$ due to relative change of nuclear data $\partial x/x$, the collision history-based method (Aufiero et al., 2015) artificially increases all cross sections (Σ_G) involved in generalized sensitivity calculations by a factor of f_a. As a result, all the reactions G are accepted by a probability of $\frac{1}{f_a}$ and rejected by a probability of $1 - \frac{1}{f_a}$. This way, the distribution of particles is unchanged. Fig. 1 shows a neutron history of unperturbed system after all cross sections are increased by a factor of $f_a = 2$.

With accepted and rejected events, one can consider perturbation in neutron weight with the same neutron tracks as an unperturbed system by using biased sampling. The basic idea is quite similar to correlated sampling method (Bernnat, 1974; Nagaya, 2012). Assuming $p(S)$ is the probability density function at phase space S for the unperturbed system and $p^*(S)$ is the probability density function at phase space S for the perturbed system, one can obtain
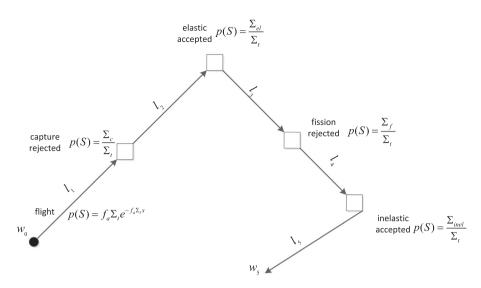
Fig. 1. Neutron history for the unperturbed system.

$$p^*(S) = \frac{p^*(S)}{p(S)} p(S) = w_f(S)p(S), \tag{11}$$

where $w_f(S)$ is a weight factor when using $p(S)$ as the biased probability density function in the perturbed system; therefore, if the neutron history in the perturbed system uses the same tracks as the unperturbed system, the neutron weight should be modified by multiplying the additional weight factor $w_f(S)$ at every track, as shown in Fig. 2, where * is used as a sign for the perturbed system.

A score for Eq. (7) for both the perturbed and unperturbed systems must be evaluated. Considering the track length l_5, a score for Eq. (7) in the unperturbed systems is

$$\langle \Psi \Sigma_1 \rangle = \Sigma_1 w_5 \int_{l_5} dr = \Sigma_1 \cdot w_5 \cdot l_5, \tag{12}$$

and a score for Eq. (7) in the perturbed systems is

$$\langle \Psi^* \Sigma_1 \rangle = \Sigma_1 w_5 \cdot \frac{\Sigma_t^* e^{-f_a^* \Sigma_t^* l_1}}{\Sigma_t e^{-f_a \Sigma_t l_1}} \frac{\frac{\Sigma_c^*}{\Sigma_t^*}}{\frac{\Sigma_c}{\Sigma_t}} \cdot \frac{\Sigma_t^* e^{-f_a^* \Sigma_t^* l_2}}{\Sigma_t e^{-f_a \Sigma_t l_2}} \frac{\frac{\Sigma_{el}^*}{\Sigma_t^*}}{\frac{\Sigma_{el}}{\Sigma_t}}$$
$$\cdot \frac{\Sigma_t^* e^{-f_a^* \Sigma_t^* l_3}}{\Sigma_t e^{-f_a \Sigma_t l_3}} \frac{\frac{\Sigma_f^*}{\Sigma_t^*}}{\frac{\Sigma_f}{\Sigma_t}} \cdot \frac{\Sigma_t^* e^{-f_a^* \Sigma_t^* l_4}}{\Sigma_t e^{-f_a \Sigma_t l_4}} \frac{\frac{\Sigma_{inel}^*}{\Sigma_t^*}}{\frac{\Sigma_{inel}}{\Sigma_t}} \cdot \int_{l_5} dx$$
$$= \Sigma_1 w_5 \cdot l_5 \cdot \frac{e^{-f_a^* \Sigma_t^* (l_1 + l_2 + l_3 + l_4)}}{e^{-f_a \Sigma_t (l_1 + l_2 + l_3 + l_{14})}} \cdot \frac{\Sigma_c^*}{\Sigma_c} \cdot \frac{\Sigma_{el}^*}{\Sigma_{el}} \cdot \frac{\Sigma_f^*}{\Sigma_f} \cdot \frac{\Sigma_{inel}^*}{\Sigma_{inel}} \tag{13}$$

By artificially enforcing $f_a^* \Sigma_t^* = f_a \Sigma_t$, one obtains

$$\langle \Psi^* \Sigma_1 \rangle = \Sigma_1 \cdot w_5 \cdot l_5 \cdot \frac{\Sigma_c^*}{\Sigma_c} \cdot \frac{\Sigma_{el}^*}{\Sigma_{el}} \cdot \frac{\Sigma_f^*}{\Sigma_f} \cdot \frac{\Sigma_{inel}^*}{\Sigma_{inel}}. \tag{14}$$

A positive increment in the cross section for the accepted collisions will increase the particle weight whereas that for the rejected collision will reduce the particle weight; therefore, the perturbations in the cross sections in Fig. 2 can be expressed as
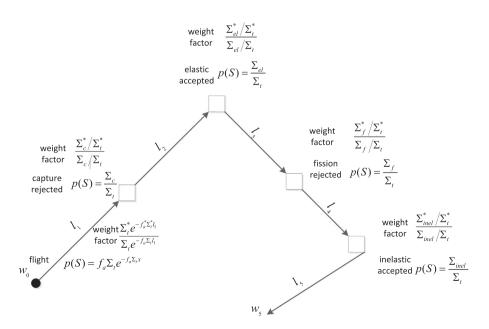

Fig. 2. Neutron history and weight perturbation approach.

$$\Sigma_c^* = \Sigma_c - \delta\Sigma_c,$$
$$\Sigma_f^* = \Sigma_f - \delta\Sigma_f,$$
$$\Sigma_{el}^* = \Sigma_{el} + \delta\Sigma_{el}, \qquad (15)$$
$$\Sigma_{inel}^* = \Sigma_{inel} + \delta\Sigma_{inel}.$$

Substituting Eq. (15) into Eq. (14), one obtains

$$\langle\Psi^*\Sigma_1\rangle = \Sigma_1 \cdot w_5 \cdot l_5 \cdot \left(1 - \frac{\delta\Sigma_c}{\Sigma_c}\right) \cdot \left(1 + \frac{\delta\Sigma_{el}}{\Sigma_{el}}\right) \cdot \left(1 - \frac{\delta\Sigma_f}{\Sigma_f}\right)$$
$$\cdot \left(1 + \frac{\delta\Sigma_{inel}}{\Sigma_{inel}}\right). \qquad (16)$$

Subtracting Eq. (12) from equation Eq. (16) and maintaining only the first order perturbation term, one obtains

$$\langle\partial\Psi\Sigma_1\rangle = \langle\Psi^*\Sigma_1\rangle - \langle\Psi\Sigma_1\rangle$$
$$\approx \Sigma_1 \cdot w_5 \cdot l_5 \cdot \left(-\frac{\delta\Sigma_c}{\Sigma_c} + \frac{\delta\Sigma_{el}}{\Sigma_{el}} - \frac{\delta\Sigma_f}{\Sigma_f} + \frac{\delta\Sigma_{inel}}{\Sigma_{inel}}\right). \qquad (17)$$

and a score for the Eq. (10) in track 5 in Fig. 2 is

$$\left\langle\frac{\partial\Psi}{\partial x}\Sigma_1 x\right\rangle$$
$$= \Sigma_1 \cdot w_5 \cdot l_5 \cdot \left(-\frac{d\Sigma_c}{dx}\cdot\frac{x}{\Sigma_c} + \frac{d\Sigma_{el}}{dx}\cdot\frac{x}{\Sigma_{el}} - \frac{d\Sigma_f}{dx}\cdot\frac{x}{\Sigma_f} + \frac{d\Sigma_{inel}}{dx}\cdot\frac{x}{\Sigma_{inel}}\right)$$
$$= \Sigma_1 \cdot w_5 \cdot l_5 \cdot \left(-\delta_{x,\Sigma_c} + \delta_{x,\Sigma_{el}} - \delta_{x,\Sigma_f} + \delta_{x,\Sigma_{inel}}\right) \qquad (18)$$

Comparing Eq. (18) with Eq. (10), it derives that

$$\frac{\partial w/w}{\partial x/x} = \sum_i \left(\delta_{x,accepted}^i - \delta_{x,rejected}^i\right), \qquad (19)$$

where i is the index of collision in the neutron history. Eq. (19) provides an algorithm, i.e., scoring accepted and rejected reactions concerning the perturbed nuclear data, to compute the perturbation in particle weight for the perturbed system with the same tracks as the unperturbed system. In order to consider the effect of source perturbation (Nagaya and Mori, 2005), the accepted and rejected events should be passed to all the progeny neutrons produced by the source neutron until the fission neutrons establish a stable population. Then Eq. (19) is modified as follows

$$\frac{\partial w/w}{\partial x/x} = \sum_{j=c}^{c-\lambda+1}\sum_{i\in j}\left(\delta_{x,accepted}^{j,i} - \delta_{x,rejected}^{j,i}\right), \qquad (20)$$

where j is the cycle index, i is the index of collision in cycle j, c is the current cycle when a score for Eq. (10) is tallied, and λ is the amount of generations or cycles used to establish an asymptotic population for the fission neutrons. Usually, a generation of ten is enough for most systems (Kiedrowski and Brown, 2013; Aufiero et al., 2015).

Substituting Eq. (20) into Eq. (10), one obtains

$$\left\langle\frac{\partial\Psi}{\partial x}\Sigma_1 x\right\rangle = \frac{1}{C_{tot}}\sum_{c=1}^{C_{tot}}\frac{1}{P_c w_0^c}\sum_{p=1}^{P_c}\sum_{\tau=1}^{L^{p,c}}\Sigma_1$$
$$\cdot \sum_{j=c}^{c-\lambda+1}\sum_{i\in j}\left(\delta_{x,accepted}^{j,i,p,c} - \delta_{x,rejected}^{j,i,p,c}\right) \cdot w_\tau^{p,c} \cdot l_\tau^{p,c}, \qquad (21)$$

where $\delta_{x,accepted}^{j,i,p,c}$ and $\delta_{x,rejected}^{j,i,p,c}$ are the value (one or zero) of accepted and rejected events of x reaction at the i-th collision of the $(c-j)$-th ancestor neutrons of the particle p in cycle c.

Implementing accepted and rejected events requires the following steps:

- Sample the flight distance l according to $l = -\ln(\xi)/\Sigma_{r_{i-1}}$, where $\Sigma_{r_{i-1}}$ is the total macroscopic cross section of the material at the current position r_{i-1}, i is the collision index, and ξ is a random number.
- Sample a collision nuclide according to probability $\Sigma_{r_{i-1}}^j / \Sigma_{r_{i-1}}$ where j is the isotope index and $\Sigma_{r_{i-1}} = \sum_j \Sigma_{r_{i-1}}^j$.
- Sample a reaction type according to probability $\sigma_{r_{i-1}}^{j,k} / \sigma_{r_{i-1}}^j$ where k is the reaction type index, and $\sigma_{r_{i-1}}^j = \sum_k \sigma_{r_{i-1}}^{j,k}$ where σ is a microscopic cross section.
- Accept the reaction type with a probability of $\frac{1}{f_a}$ and reject it with a probability of $1 - \frac{1}{f_a}$. If the reaction type is accepted, generate a positive score for Eq. (20) and update the neutron direction and energy according to the reaction type, otherwise generate a negative score for Eq. (20) and keep the neutron state unchanged. If fission occurs, pass the scores for the accepted and rejected events carried by the progenitor neutron to all its neutron progeny.
- Update position and repeat steps 1–4 in the new position $r_i = r_{i-1} + l$.

3. Superhistory algorithm for the collision history-based method

As discussed in Section 2, in order to consider the effect of fission source perturbation, the scores of accepted and rejected events for the source neutrons should be passed to all their neutron progeny for sufficient generations (e.g., 10) once the fission neutrons establish a stable population. As a result, the size of tallies to store the accepted and rejected events are proportional to the number of particle histories per cycle, and calculating numerous generalized sensitivity coefficients for a large number of isotopes and reaction types on a fined energy bins may require considerable memory consumptions. In order to reduce such huge memory requirements, different algorithms have been put forward. For example, MCNP6 uses a sparse data handling scheme (Kiedrowski and Brown, 2013) based on the fact that not every particle produces a progeny. Another example, McCARD uses adjoint Wielandt algorithm in which the pedigree of a single history is utilized by applying the MC Wielandt method (Choi and Shim, 2015). A third example, SERPENT2 stores the information (collision nuclide, reaction type, neutron energy and whether this reaction is accepted or rejected) of every collision point and calculates the accepted and rejected events only when having a score for Eq. (21), i.e. at the asymptotic generation, rather than having a direct score for the perturbed nuclear data at every collision point before the fission neutrons establish a stable population. The memory consumption of the collision history-based method may be expensive due to the power iteration process and to the fact that particles in the following cycles can be simulated only when all particles in a cycle die. The particle simulation procedure in the power iteration process is shown in Fig. 3, where g means cycle or generation. As a result, if any information needs to be passed to the progeny, the tally size to store the information would be proportional to the number of particle histories in every cycle.

In this work, an algorithm for the collision history-based method, namely, the superhistory algorithm, is applied in the RMC code to further reduce memory consumption of the collision history-based method. By reducing the frequencies of source renormalization, the superhistory method was first used to decrease the biases of effective multiplication factor and flux distributions (Brissenden and Garlick, 1986), but it can be also applied to source convergence acceleration (Blomquist and Gelbard, 2002; She et al., 2012). In the superhistory method, a source neutron and all its progeny neutrons are tracked for a number of generations, called a
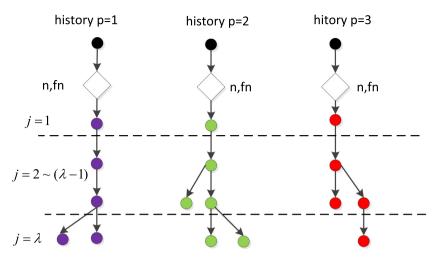
Fig. 3. Process of power iteration method.

supergeneration, before any fission neutrons are stored into the fission neutron bank for the next cycle. The history of a source neutron and all its progeny before being stored in the fission bank is called a superhistory, which has a pedigree of ordinary fission-to-fission histories. The particle simulation procedure in the superhistory method is shown in Fig. 4. Superhistories are simulated one by one and information on all previous neutrons are obtained within each superhistory rather than waiting for the end of all cycles.

The superhistory algorithm modifies Eq. (21) as follows

$$
\left\langle \frac{\partial \Psi}{\partial x} \Sigma_1 x \right\rangle = \frac{1}{C_{tot}} \sum_{c=1}^{C_{tot}} \frac{1}{P_c} \sum_{p=1}^{P_c} \frac{1}{Q^{\lambda,p,c} w_0^{\lambda,p,c}} \sum_{q=1}^{Q^{\lambda,p,c}} \sum_{\tau=1}^{L^{q,\lambda,p,c}} \Sigma_1
$$
$$
\cdot \frac{\partial w_\tau^{q,\lambda,p,c}/w_\tau^{q,\lambda,p,c}}{\partial x/x} \cdot w_\tau^{q,\lambda,p,c} \cdot l_\tau^{q,\lambda,p,c}
$$
$$
= \frac{1}{C_{tot}} \sum_{c=1}^{C_{tot}} \frac{1}{P_c} \sum_{p=1}^{P_c} \frac{1}{Q^{\lambda,p,c} w_0^{\lambda,p,c}} \sum_{q=1}^{Q^{\lambda,p,c}} \sum_{\tau=1}^{L^{q,\lambda,p,c}} \Sigma_1
$$
$$
\cdot \sum_{j=0}^{\lambda-1} \sum_{i\in j} \left(\delta_{x,accepted}^{j,i,q,\lambda,p,c} - \delta_{x,rejected}^{j,i,q,\lambda,p,c} \right) \cdot w_\tau^{q,\lambda,p,c} \cdot l_\tau^{q,\lambda,p,c}. \quad (22)
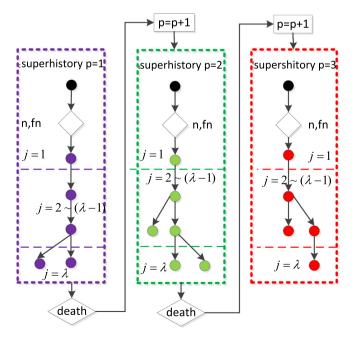$$

Fig. 4. Process of superhistory method.

where c is cycle index, C_{tot} is the total number of active cycles, p is superhistory index in cycle c, P_c is the total number of superhistories in cycle c, where λ is the value of supergeneration and in this work it also represents the amount of generations used to establish an asymptotic population for the fission neutrons, $Q^{\lambda,p,c}$ is the total number of neutrons in the supergeneration in superhistory p in cycle c, $w_0^{\lambda,p,c}$ is initial weight of every particle in the supergeneration in superhistory p in cycle c, τ is track index for particle q in the supergeneration in superhistory p in cycle c, $L^{q,\lambda,p,c}$ is total number of tracks for particle q in the supergeneration in superhistory p in cycle c, $w_\tau^{q,\lambda,p,c}$ and $l_\tau^{q,\lambda,p,c}$ are the current weight and track length of particle q at track τ in the supergeneration in superhistory p in cycle c, and $\delta_{x,accepted}^{j,i,q,\lambda,p,c}$ and $\delta_{x,rejected}^{j,i,q,\lambda,p,c}$ are the value (one or zero) of accepted and rejected events of x reaction at the i-th collision of the j-th ancestor neutrons of the particle q in the supergeneration in superhistory p in cycle c.

The memory requirement used to store accepted and rejected events is proportional to the expected number of fission points caused by a single particle history rather than the number of particle histories in every cycle. Assuming that for critical systems $\overline{Q^{\lambda,p,c}} = 1$, which means the average number of fission neutrons caused by a source neutron is one, the memory requirement for the superhistory algorithm is much smaller than that for the power iteration method. However, it should be noted that the superhistory algorithm represents a compromise between memory consumption and computational efficiency (theoretically, it should be as efficient as MCNP6 which adopts the non-overlapping blocks algorithm) since sensitivity coefficients can only be computed at specific generations, i.e. at the supergenerations, whereas the multiple overlapping algorithms implemented in SERPENT2 may be more efficient than the superhistory algorithm by a factor of λ (where λ is the amount of generations or cycles used to establish an asymptotic population for the fission neutrons) assuming every cycle can have a score for sensitivity coefficients.

4. Verification and results

In this work, the superhistory algorithm was used to implement the collision history-based method into the continuous-energy Reactor Monte Carlo (RMC) code developed by Tsinghua University, Beijing, China (Wang et al., 2015) for reducing memory consumption of calculating generalized sensitivity coefficients. The newly developed capability of RMC was verified by comparing with results computed by TSUNAMI-1D in SCALE6.1 (Oak Ridge

National Laboratory, 2011) and SERPENT2 (Aufiero et al., 2015) in three different benchmark problems: Jezebel, Flattop and the UAM TMI PWR pin cell. All the calculations performed by RMC are on the Inspur TS10000 HPC Server, the Tsinghua Performance Computational Platform with 740 nodes. Each node has 12 CPUs (Intel Xeon X5670 at 2.93 GHz) sharing 32 gigabytes or 48 gigabytes of memory. All calculations performed by RMC and SERPENT2 are in continuous-energy mode based on the ENDF/B-VII nuclear data library whereas TSUNAMI-1D calculations used the 238 groups cross-section library based on ENDF/B-VII nuclear data library. For consistency, the same response function (referred to as F28/F25 from now on)

$$
R = \frac{\iiint \sum_{f}^{238U}(r, E)\Psi(r, E, \Omega)dEdrd\Omega}{\iiint \sum_{f}^{235U}(r, E)\Psi(r, E, \Omega)dEdrd\Omega}, \tag{23}
$$

where Σ_f^{238U} and Σ_f^{235U} represent fission cross section for U-238 and U-235 respectively,was chosen for all the three problems even though all the three codes can perform different types of linear response functions and SERPENT2 can also compute bilinear response functions (Aufiero et al., 2015) in the form of flux and adjoint flux. In RMC calculations, for evaluating the impact of perturbed fission source, the perturbation of the particle weight is computed by looking back into ten generations, meaning that the asymptotic generation is set to be ten.

4.1. Jezebel benchmark

The Jezebel (NEA Nuclear Science Committee, 2011) benchmark consists of a bare sphere of plutonium. Sensitivity coefficients, for comparison with TSUNAMI-1D and SERPENT2, were evaluated for five isotopes using a 175-group structure (Aufiero et al., 2015). The response function was calculated in a central sphere of 1-cm

Table 1
Energy integrated sensitivity coefficients of the response function F28/F25 for the Jezebel benchmark.
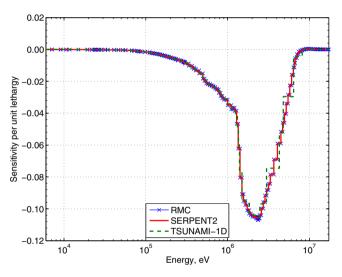
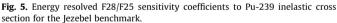| Nuclide	Nuclear data	RMC		TSUNAMI-1D	Relative difference (%)
		F28/F25	RSD (%)	F28/F25	
Pu-239	Inelastic	−1.601E−01	0.06	−1.588E−01	0.77
Pu-239	n,2n	−1.986E−03	0.33	−1.964E−03	1.10
Pu-239	Fission	5.181E−02	0.15	5.004E−02	3.54
Pu-239	n,gamma	1.007E−02	0.13	1.006E−02	0.11
Pu-239	Elastic	−6.410E−02	0.25	−6.380E−02	0.47
Pu-239	Disappear	1.007E−02	0.13	1.006E−02	0.11
Pu-239	Total	−1.643E−01	0.12	−1.645E−01	−0.15
Pu-240	nubar	−1.806E−03	1.29	−1.829E−03	−1.26
Pu-240	Elastic	−4.082E−03	0.91	−4.077E−03	0.12
Pu-240	Inelastic	−8.036E−03	0.26	−7.984E−03	0.66
Pu-240	n,2n	−6.811E−05	1.79	−6.654E−05	2.36
Pu-240	Fission	−2.534E−03	1.04	−2.559E−03	−0.98
Pu-240	n,gamma	6.247E−04	0.57	6.139E−04	1.75
Pu-240	Disappear	6.247E−04	0.57	6.139E−04	1.75
Pu-240	Total	−1.410E−02	0.36	−1.407E−02	0.16
Pu-241	Elastic	−1.407E−04	6.30	−1.426E−04	−1.30
Pu-241	Inelastic	−6.156E−04	0.92	−6.056E−04	1.65
Pu-241	n,2n	−3.733E−05	2.30	−3.657E−05	2.08
Pu-241	Fission	8.172E−05	9.73	6.889E−05	18.62
Pu-241	n,gamma	4.051E−05	2.36	3.915E−05	3.47
Pu-241	nubar	−1.429E−04	4.94	−1.538E−04	−7.14
Pu-241	Disappear	4.051E−05	2.36	3.915E−05	3.47
Pu-241	Total	−6.714E−04	1.97	−6.767E−04	−0.77
Ga-69	Elastic	−1.731E−03	1.19	−1.746E−03	−0.84
Ga-71	Disappear	3.825E−05	2.17	3.624E−05	5.53

radius. The energy-resolved F28/F25 sensitivity coefficients for the Jezebel problem computed by RMC and TSUNAMI-1D are presented in Table 1. Relative differences between RMC and TSUNAMI-1D are within 3–5% for most of the nuclear data, indicating RMC generally agrees with TSUNAMI-1D. The largest difference between RMC and TSUNAMI-1D lies in the Pu-240 fission cross section where a difference of 18.62% is observed. The significant difference is due to the large relative standard deviation of RMC, i.e., 9.73%.

Figs. 5, 7 and 9 show that the energy-resolved F28/F25 sensitivity coefficients with regard to Pu-249 inelastic cross section, Pu-249 elastic cross section, and Pu-249 total chi, respectively, agree very well among RMC, SERPENT2 and TSUNAMI-1D. Moreover, Figs. 6, 8 and 10 show that in general the difference between RMC and SERPENT2 is within three standard deviations of RMC sensitivities.

4.2. Flattop benchmark

The Flattop (NEA Nuclear Science Committee, 2011) benchmark is a sphere of delta-phase plutonium reflected by an annulus of
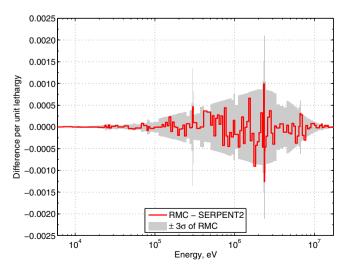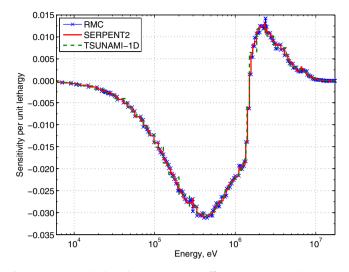
Fig. 5. Energy resolved F28/F25 sensitivity coefficients to Pu-239 inelastic cross section for the Jezebel benchmark.

Fig. 6. Difference of energy resolved F28/F25 sensitivity coefficients to Pu-239 inelastic cross section for the Jezebel benchmark.

Fig. 7. Energy resolved F28/F25 sensitivity coefficients to Pu-239 elastic cross section for the Jezebel benchmark.
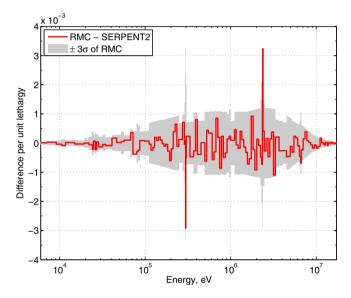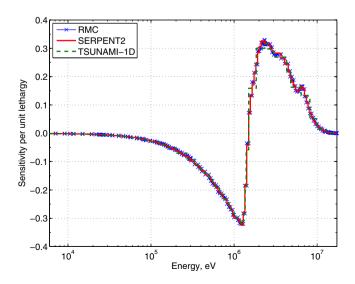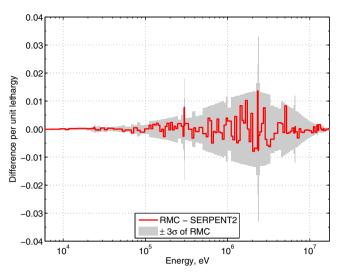

Fig. 10. Difference of energy resolved F28/F25 sensitivity coefficients to Pu-239 total chi for the Jezebel benchmark.

Fig. 8. Difference of energy resolved F28/F25 sensitivity coefficients to Pu-239 elastic cross section for the Jezebel benchmark.

Fig. 9. Energy resolved F28/F25 sensitivity coefficients to Pu-239 total chi for the Jezebel benchmark.

normal uranium. As in the previous case a 175 group structure was used for evaluating the sensitivity coefficients and the response function was calculated in a central sphere of 1-cm radius for eight different isotopes. The energy-resolved F28/F25 sensitivity coefficients for the Flattop problem computed by RMC, SERPENT2 and TSUNAMI-1D are presented in Table 2. The relative differences between RMC and SERPENT are within 4%, whereas the relative differences between RMC and TSUNAMI-1D are within 6%, indicating RMC is in better agreement with SERPENT than with TSUNAMI-1D. Figs. 11, 13 and 15, show that the energy-resolved F28/F25 sensitivity coefficients with regard to Pu-239 fission cross section, Pu-239 chi and U-235 nubar, respectively, agree well among RMC, SERPENT2 and TSUNAMI-1D, whereas Figs. 12, 14 and 16 show that the differences between RMC and SERPENT2 are mostly within three standard deviations of RMC sensitivities.

4.3. UAM TMI PWR pin cell benchmark

The UAM TMI PWR pin cell problem is the Exercise 1 (I–1) in the Phase I of the OECD LWR UAM benchmarks (Ivanova et al., 2013). In this case a 238 group structure was used to calculate sensitivity coefficients for a total of 34 different isotopes, and the response function was evaluated in the whole fuel pellet volume. The energy-resolved F28/F25 sensitivity coefficients for the UAM TMI PWR pin cell benchmark computed by RMC and TSUNAMI-1D are presented in Table 3. The relative differences between RMC and TSUNAMI-1D are within 9%. Figs. 17, 19, 21 and 23 show the energy-resolved F28/F25 sensitivity coefficients with regard to H-1 total cross section, Hf disappearance cross section, U-238 disappearance cross section, and O-16 elastic cross section, respectively. Figs. 18, 20, 22 and 24 show the differences among the three codes with regard to the same four nuclear data. In general, the F28/F25 sensitivity coefficient profiles among RMC, SERPENT2 and TSUNAMI-1D agree well. However, some differences between RMC and TSUNAMI-1D can be observed in the energy range between 10^6 eV and 10^7 eV (Fig. 23). Differences between RMC and SERPENT2 are roughly within three standard deviations of RMC sensitivities, the differences between the two Monte Carlo codes and TSUNAMI-1D, instead, are much larger, i.e., up to 50% relative difference in the sensitivity estimates. This behavior may be attributed to the fact that TSUNAMI-1D used the 238 multi-group nuclear data library whereas RMC used the continuous-energy nuclear data library.

Table 2
Energy integrated sensitivity coefficients of the response function F28/F25 for the Flattop benchmark.

Nuclide	Nuclear Data	RMC		SERPENT2		TSUNAMI-1D	RMC-SERPENT2 relative difference (%)	RMC-TSUNAMI relative difference (%)
		F28/F25	RSD (%)	F28/F25	RSD (%)			
Pu-239	nubar	5.671E−02	0.14	5.680E−02	0.11	5.528E−02	−0.16	2.60
Pu-239	Inelastic	−1.137E−01	0.13	−1.138E−01	0.10	−1.136E−01	−0.13	0.11
Pu-239	n,2n	−1.445E−03	0.66	−1.465E−03	0.48	−1.364E−03	−1.35	5.95
Pu-239	Fission	1.728E−01	0.09	1.726E−01	0.07	1.720E−01	0.12	0.51
Pu-239	Elastic	−1.409E−02	2.13	−1.462E−02	1.56	−1.396E−02	−3.63	0.91
Pu-239	Disappear	1.860E−02	0.16	1.847E−02	0.12	1.908E−02	0.75	−2.47
Pu-239	Total	6.219E−02	0.60	6.114E−02	0.47	6.211E−02	1.72	0.13
Pu-240	Elastic	−1.252E−03	5.75	−1.260E−03	4.37	−1.218E−03	−0.64	2.81
Pu-240	Inelastic	−6.171E−03	0.55	−6.200E−03	0.00	−6.145E−03	−0.48	0.42
Pu-240	Disappear	1.253E−03	0.61	1.200E−03	0.00	1.270E−03	4.39	−1.32
Pu-240	Total	−5.648E−03	1.60	−5.800E−03	1.72	−5.580E−03	−2.63	1.20
U-235	Inelastic	−4.853E−04	3.48	−4.890E−04	2.66	−4.881E−04	−0.76	−0.58
U-235	Fission	−1.005E+00	0.00	−1.004E+00	0.00	−1.005E+00	0.01	0.00
U-235	nubar	−7.529E−03	0.30	−7.486E−03	0.24	−7.619E−03	0.58	−1.18
U-235	Disappear	6.183E−04	0.90	6.170E−04	0.65	6.418E−04	0.20	−3.67
U-235	Total	−1.005E+00	0.01	−1.005E+00	0.00	−1.005E+00	−0.01	−0.01
U-238	Elastic	−1.256E−01	0.41	−1.254E−01	0.31	−1.246E−01	0.14	0.79
U-238	Inelastic	−8.000E−02	0.28	−8.017E−02	0.21	−8.043E−02	−0.21	−0.53
U-238	n,2n	−1.242E−03	1.24	−1.267E−03	0.95	−1.241E−03	−2.00	0.02
U-238	Fission	9.655E−01	0.01	9.654E−01	0.01	9.655E−01	0.01	0.00
U-238	nubar	−4.968E−02	0.13	−4.973E−02	0.11	−4.975E−02	−0.08	−0.14
U-238	Disappear	4.440E−02	0.14	4.417E−02	0.10	4.520E−02	0.52	−1.76
U-238	Total	8.030E−01	0.07	8.027E−01	0.05	8.044E−01	0.04	−0.17

Fig. 11. Energy resolved F28/F25 sensitivity coefficients to Pu-239 fission cross section for the Flattop benchmark.
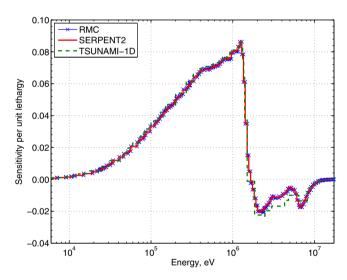

Fig. 12. Difference of energy resolved F28/F25 sensitivity coefficients to Pu-239 fission cross section for the Flattop benchmark.

4.4. Memory consumption

The memory consumptions of the superhistory algorithm and the normal algorithm which is implemented in the power iteration process (power method) for the Jezebel, Flattop and the UAM TMI PWR pin cell benchmarks are summarized in Table 4. The memory consumption of the superhistory algorithm for the Jezebel, Flattop and the UAM TMI PWR pin cell problems are only 0.38%, 0.47%, 0.14% of that of the normal algorithm, respectively. This suggests that the superhistory algorithm consumes much less memory than the normal algorithm. It should be noted that the normal algorithm is not optimized, meaning it does not use memory reducing schemes like MCNP6 or SERPENT2. The computational time is not addressed in this work. Nevertheless, it could be inferred that the efficiency of the superhistory algorithm would be similar to the normal algorithm with only one particle history per cycle.
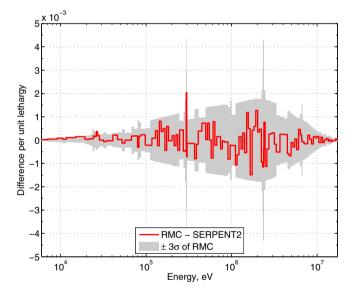
5. Conclusions

A new feature for generalized sensitivity analysis with regard to nuclear data was developed in the continuous-energy Monte Carlo code RMC (Reactor Monte Carlo). This new capability relies on the collision history-based method that was previously implemented in SERPENT2, and uses the superhistory algorithm in order to reduce the memory consumption when computing generalized sensitivity coefficients. The newly developed capability of RMC was verified by comparing with results from the deterministic code TSUNAMI-1D part of the SCALE6.1 code package, and the Monte Carlo code SERPENT2, through Jezebel, Flattop and the UAM TMI PWR pin cell benchmark problems. Numerical results show that RMC, SERPENT2 and TSUNAMI-1D reach a good agreement generally, although the differences between the Monte Carlo codes and
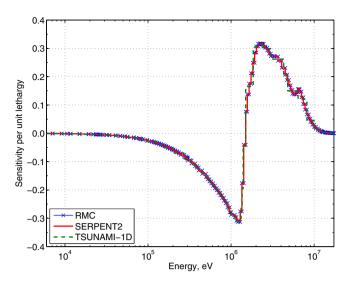
Fig. 13. Energy resolved F28/F25 sensitivity coefficients to Pu-239 total chi for the Flattop benchmark.
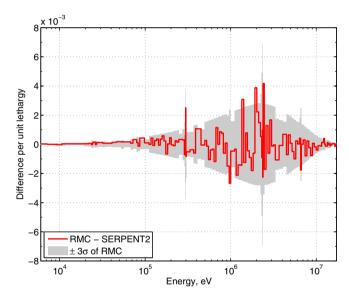

Fig. 14. Difference of energy resolved F28/F25 sensitivity coefficients to Pu-239 total chi for the Flattop benchmark.
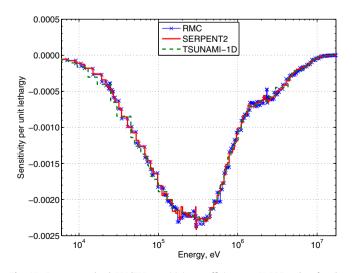

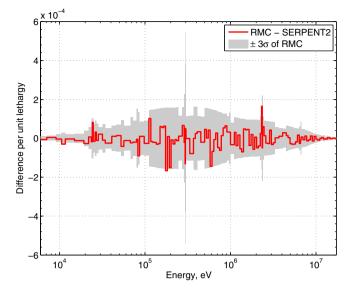**Fig. 15.** Energy resolved F28/F25 sensitivity coefficients to U-235 nubar for the Flattop benchmark.

Fig. 16. Difference of energy resolved F28/F25 sensitivity coefficients to U-235 nubar for the Flattop benchmark.

Table 3
Energy integrated sensitivity coefficients for the UAM TMI PWR pin cell benchmark for the response function F28/F25.

| Nuclide | Nuclear data | RMC | | TSUNAMI-1D | Relative difference (%) |
		F28/F25	RSD (%)	F28/F25	
U-234	Inelastic	−6.686E−05	5.28	−6.499E−05	−2.87
U-234	n,2n	−5.780E−07	24.78	−5.604E−07	−3.15
U-234	n,gamma	3.678E−03	0.38	3.385E−03	−8.64
U-235	Inelastic	−8.428E−03	0.44	−8.373E−03	−0.66
U-235	n,2n	−2.995E−04	1.13	−2.949E−04	−1.54
U-235	Fission	−2.754E−01	0.09	−2.759E−01	0.21
U-235	n,gamma	1.629E−01	0.06	1.641E−01	0.74
U-235	Total	−1.213E−01	0.26	−1.203E−01	−0.81
U-238	Inelastic	−2.181E−01	0.08	−2.171E−01	−0.46
U-238	n,2n	−7.826E−03	0.22	−7.902E−03	0.97
U-238	Fission	9.729E−03	0.01	9.733E−03	0.04
U-238	n,gamma	2.047E−01	0.06	2.219E−01	7.76
U-238	nubar	−1.835E−03	2.76	−1.849E−03	0.75
U-238	Total	9.437E−01	0.06	9.511E−01	0.77
O-16	Elastic	−7.715E−02	0.87	−7.881E−02	2.11
O-16	n,alpha	−6.159E−03	0.24	−6.042E−03	−1.94
O-16	Inelastic	−5.747E−03	0.27	−5.821E−03	1.27
O-16	Disappear	−6.159E−03	0.24	−6.093E−03	−1.09
O-16	Total	−8.906E−02	0.76	−9.080E−02	1.92
H-1	Disappear	4.094E−02	0.11	4.045E−02	−1.21
H-1	Total	−6.681E−01	0.11	−6.831E−01	2.19
Cr-53	n,gamma	5.552E−05	2.89	5.510E−05	−0.75
Fe-56	n,gamma	1.503E−04	1.79	1.528E−04	1.60
Zr-90	n,gamma	1.284E−03	0.64	1.206E−03	−6.49
Zr-91	n,gamma	4.308E−03	0.34	4.505E−03	4.36
Sn-117	n,gamma	1.097E−04	2.11	1.110E−04	1.17
Hf-177	Total	4.837E−04	1.10	4.706E−04	−2.78
Hf-179	n,gamma	2.611E−05	4.28	2.602E−05	−0.35

TSUNAMI-1D are larger than the differences between RMC and SERPENT2, which may be attributed to the fact that TSUNAMI-1D used the 238 multi-group nuclear data library whereas RMC and SERPENT2 used the continuous-energy nuclear data library. The superhistory algorithm applied for the collision history-based method is effective in reducing memory consumption. Future work will focus on extending the capabilities of computing sensitivity coefficients to bilinear ratios (Aufiero et al., 2015) and apply the generalized sensitivity coefficients to uncertainty propagation in depletion calculations (Park et al., 2011).
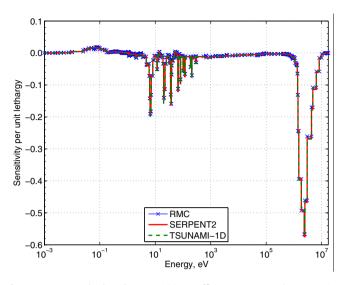
Fig. 17. Energy resolved F28/F25 sensitivity coefficients to H-1 total cross section for the UAM TMI PWR pin cell benchmark.
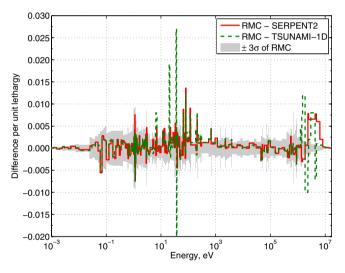

Fig. 18. Difference of energy resolved F28/F25 sensitivity coefficients to H-1 total cross section for the UAM TMI PWR pin cell benchmark.
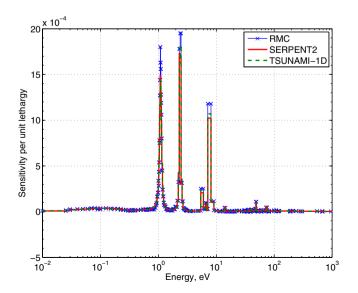

Fig. 19. Energy resolved F28/F25 sensitivity coefficients to Hf disappearance cross section for the UAM TMI PWR pin cell benchmark.
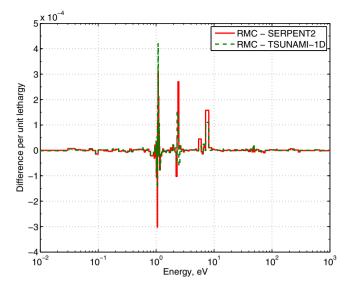

Fig. 20. Difference of energy resolved F28/F25 sensitivity coefficients to Hf disappear cross section for the UAM TMI PWR pin cell benchmark.
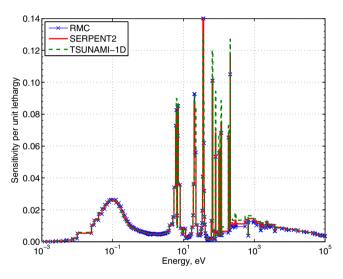

Fig. 21. Energy resolved F28/F25 sensitivity coefficients to U-238 disappear cross section for the UAM TMI PWR pin cell benchmark.
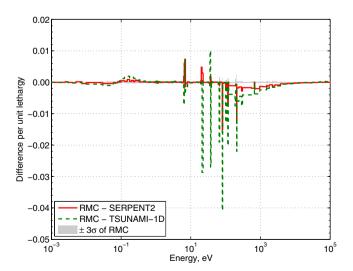

Fig. 22. Difference of energy resolved F28/F25 sensitivity coefficients to U-238 disappear cross section for the UAM TMI PWR pin cell benchmark.
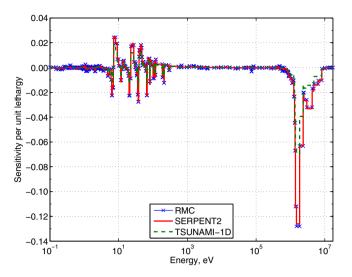
Fig. 23. Energy resolved F28/F25 sensitivity coefficients to O-16 elastic cross section for the UAM TMI PWR pin cell benchmark.
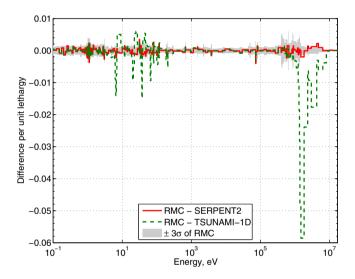

Fig. 24. Difference of energy resolved F28/F25 sensitivity coefficients to O-16 elastic cross section for the UAM TMI PWR pin cell benchmark.

Table 4
Comparison of memory consumption of different algorithms.

Problem	Normal algorithm	Superhistory algorithm	Superhistory-to-normal ratio
Jezebel	2.8G	10.6 M	0.00379
Flattop	8.1G	38.2 M	0.00472
Pin cell	33.0G	46.5 M	0.00141

References

Aufiero, M., Bidaud, A., Hursin, M., 2015. A collision history-based approach to sensitivity/perturbation calculations in the continuous energy Monte Carlo code SERPENT. Ann. Nucl. Energy 85, 245–258.

Baker, C., Smith, P.N., Mason, R., et al., 2015. Calculating Uncertainty on k-effective with Monk 10. In: ICNC 2015, Charlotte, NC, September 13-17, 2015.

Bernnat, W., 1974. A Monte Carlo Technique for Local Perturbations in Multiplying Systems ANL-75-2, 261–279.

Blomquist, R.N., Gelbard, E.M., 2002. Alternative implementations of the Monte Carlo power method. Nucl. Sci. Eng. 141, 85–100.

Brissenden, R.J., Garlick, A.R., 1986. Biases in the estimation of keff and its error by Monte Carlo methods. Ann. Nucl. Energy 113, 63–83.

Choi, S.H., Shim, H.J., 2015. Adjoint sensitivity and uncertainty analysis in Monte Carlo Wielandt calculations. In: ANS MC2015 – Joint International Conference on Mathematics and Computation (M&C), Supercomputing in Nuclear Applications (SNA) and the Monte Carlo (MC) Method, Nashville, TN, April 19–23 (2015).

Ivanova, K., Avramova, M., Kamerow, S., et al., 2013. Benchmark For Uncertainty Analysis in Modeling (UAM) For Design. Operation and Safety Analysis of LWRs, NEA/NSC/DOC, p. 2013.

Jinaphanh, A., Leclaire, N., Cochet, B., Quaghebeur, B., 2015. Validation of continuous energy sensitivity coefficients calculations in the MORET 5 code, ICNC 2015, Charlotte, NC, September 13-17, 2015.

Kiedrowski, B.C., Brown, F.B., 2013. Adjoint-based k-eigenvalue sensitivity coefficients to nuclear data using continuous-energy Monte Carlo. Nucl. Sci. Eng. 174, 227–244.

Nagaya, Y., Mori, T., 2005. Impact of perturbed fission source on the effective multiplication factor in Monte Carlo perturbation calculations. J. Nucl. Sci. Technol. 42 (5), 428–441.

Nagaya, Y., 2012. Monte carlo perturbation methods: sampling techniques and fission source perturbation. In: Workshop on the Advanced Monte Carlo Methodology at Seoul National University, Seoul, Korea, December 17-18 2012.

NEA Nuclear Science Committee, 2011. International Handbook of Evaluated Criticality Safety Benchmarks Experiments. OECD Nuclear Energy Agency.

Park, H.J., Shim, H.J., Kim, C.H., 2011. Uncertainty propagation in Monte Carlo depletion analysis. Nucl. Sci. Eng. 167, 196–208.

Perfetti, C.M., Rearden, B.T., 2013. Continuous-energy Eigenvalue sensitivity coefficient calculations in TSUNAMI-3D, International Conference on Mathematics and Computational Methods Applied to Nuclear Science & Engineering (M&C 2013), Sun Valley, Idaho, USA, May 5-9, 2013. CD-ROM, American Nuclear Society, LaGrange Park, IL.

Perfetti, C.M., Rearden, B.T., 2014. Continuous-Energy Monte Carlo Methods for Calculating Generalized Response Sensitivities Using TSUNAMI-3D. Proc. PHYSOR 2014, The Westin Miyako, Kyoto, Japan, September 28 – October 3, on CD-ROM (2014).

Qiu, Y., Liang, J., Wang, K., Yu, J., 2015. New strategies of sensitivity analysis capabilities in continuous-energy Monte Carlo code RMC. Ann. Nucl. Energy 81, 50–61.

Qiu, Y., Shang, X., Tang, X., Liang, J., Wang, K., 2016. Computing eigenvalue sensitivity coefficients to nuclear data by adjoint superhistory method and adjoint Wielandt method implemented in RMC code. Ann. Nucl. Energy 87, 228–241.

SCALE: A Comprehensive Modeling and Simulation Suite for Nuclear Safety Analysis and Design, ORNL/TM-2005/39, Version 6.1, 2011. Oak Ridge National Laboratory, Oak Ridge, Tennessee. Available from Radiation Safety Information Computational Center at Oak Ridge National Laboratory as CCC-785.

She, D., Wang, K., Yu, G., 2012. Asymptotic Wielandt method and superhistory method for source convergence in Monte Carlo criticality calculation. Nucl. Sci. Eng. 172, 127–137.

Shim, H.J., Kim, C.H., 2011. Adjoint sensitivity and uncertainty analyses in Monte Carlo forward calculations. J. Nucl. Sci. Technol. 05, 1453–1461.

Truchet, G., Leconte, P., Santamarina, A., 2015. Implementation and validation of reference sensitivity profile calculations in TRIPOLI4, ICNC 2015, Charlotte, NC, September 13-17, 2015.

Wang, K., Li, Z., She, D., et al., 2015. RMC – a Monte Carlo code for reactor core analysis. Ann. Nucl. Energy 82, 121–129.

X-5 Monte Carlo Team, 2003. MCNP – A General Monte Carlo N-Particle Transport Code, Version 5, Volume I: Overview and Theory, Tech. Rep., LA-UR-03-1987. Los Alamos National Laboratory.